Progress In Electromagnetics Research B, Vol. 60, 241–258, 2014

Test Dipole Selection for Linear Sampling in Transverse Electric Case

Krishna Agarwal*

Abstract—This paper discusses the problem of choosing an appropriate direction of the test dipole used in linear sampling for the 2-dimensional inverse scattering problem of the transverse electric case. In particular, we propose two approaches, one purely mathematical and the other based on the physics theory of multipole expansion of the scattered magnetic field. It is shown that though the approaches are drawn from different perspectives, they perform similarly and show reasonable reconstruction for several interesting and difficult to reconstruct dielectric scatterers.

1. INTRODUCTION

Linear sampling method (LSM) is a qualitative reconstruction technique for inverse scattering problems [1–15] such as ground penetrating radar and biomedical imaging using microwaves [16, 17]. Instead of using non-linear scattering operator, LSM uses a simplified linear mathematical model suitable for detecting the scatterer support. Several works have strengthened the mathematical theory of LSM by providing physical insights and engineering modifications [18–26]. Recently, physical connections between the linear model of LSM and non-linear model of scattering have been studied for the scalar electromagnetic scattering problem (i.e., the s-polarization or transverse magnetic (TM) two-dimensional scattering problem of dielectric scatterers) [19–22]. It has been shown that the hypothetical fundamental test source at the sampling point used in the LSM is closely related to the induced current distribution on the scatterer support and its effective multipole expansion at the sampling point.

The transverse electric (TE) inverse scattering problem of dielectric scatterers, which is a vectorial inverse scattering problem, is the focus of the current work. The vectorial inverse scattering problem poses an important challenge for LSM. As opposed to the presence of only a scalar monopole induced current in TM case, the induced current at any scatterer location is a vector dipole current in the TE case [4]. Consequently, when using LSM, we need to choose a direction for the hypothetical test dipole. However, in our knowledge, current state of research on LSM offers no technique to choose a suitable direction of the test dipole. Most researchers recommend that the images can be first obtained using dipoles along the co-ordinate axes (i.e., x, y, z-axes in 3-dimensional case and x and y axes in 2-dimensional case) and later super-imposed to get an effective image [4, 27]. The hope is that at least one of the co-ordinate axis may result into a detection of the scatterer. Though this concept works well in general, the images obtained demonstrate severe directional effects. On the other hand, it is obvious that for each sampling point, the most suitable direction of the test dipole may not be along the coordinate axis but a particular combination of the dipoles along the coordinate axes. It is also reasonable that the direction of the most suitable test dipole may vary from one sampling point to another. An interesting example is presented in Section 2.3 to illustrate the effect of the suitable test dipole.

While the importance of the most suitable test dipole is clear, it is notable that determining the most suitable test dipole is very difficult for the case of extended scatterers. Earlier, it was shown that an

Received 27 May 2014, Accepted 5 August 2014, Scheduled 10 August 2014

* Corresponding author: Krishna Agarwal (uthkrishth@gmail.com).
The author is with the Department of Electrical and Computer Engineering, National University of Singapore, Singapore 117576, Singapore.

optimal direction of the test dipole used in multiple signal classification (MUSIC) can be uniquely and analytically determined for two-dimensional TE problem of point-like scatterers [28], and interestingly the optimal test dipole matches with the actual induced dipole quite closely for the anisotropic scatterers. Such selection is possible for MUSIC because MUSIC uses rank deficiency of the multi-static response matrix $\mathbf{K}$ which happens when the number of independent induced sources is less than the number of independent measurements. This property is absent in the case of extended scatterers since extended scatterers have an induced current distribution unlike the finite number of independent induces sources on point-like scatterers.

This paper presents two methods for automatic determination of the direction of the test dipole used in LSM. The first method is based on using the scattered field data to identify a numerically stable component of the effective induced current dipole at a sampling point, which can be used as an automatic test dipole direction. The method used is similar to the stable test direction estimation proposed in [29] for the problem of detecting few point-like scatterers using MUSIC. Though the mathematical structure is similar, the physical implications are different for MUSIC and LSM, which are discussed in Section 3.2.

The second method uses multipole expansion theory for determining the direction of the test dipole. Though the general theory of multipole expansion similar to [21, 22] is still directly applicable, the nature of induced current distribution is quite different in the vectorial case as compared to the scalar case. The dipole current in the vectorial case is a vector and for the same scatterer profile, it is much weaker than the monopole current induced in the scalar case. Since the strength of the monopole currents is large in the scalar case, the multipole expansion of the induced current distribution at a scattering location still has the monopole as the most significant contributor. However, in the vectorial problem, since the induced dipole currents are not sufficiently large, the multipole expansion of the induced current distribution at a scattering location may indicate that the dipole components are not the strongest components of the multipole expansion. Thus, a strict normalization used in [21] (that includes only monopole and dipole components) is not applicable here.

Both the methods are tested for several difficult shapes of dielectric scatterers in noise levels up to 10 dB signal to noise ratio SNR (defined as $20\log_{10}(\|\mathbf{K}\|/\|\kappa\|)$, where κ denotes the noise matrix corresponding to additive Gaussian noise and $\|\cdot\|$ indicates the Frobenius norm). While the reconstruction results of both the methods are encouraging in general, it might be possible to improve their performance by designing better schemes for choosing the regularization parameters. Our aim in presenting these methods is to provide two different perspective into the operator used in linear sampling method. The first perspective is that though it might be difficult to determine an optimal direction of the test dipole in the case of LSM, a numerically suitable (for example in terms of the stability) test dipole or a physics based (using multipole expansion) test dipole may serve a better purpose in applying LSM for a variety of scatterers, including scatterers with strong dimensionality. The second perspective is that possibly there are some unexplored links between the mathematical model of linear sampling and the actual physical phenomenon of scattering, which may provide more insight and more useful tools in the application of LSM.

The outline of the paper is as follows. Section 2 introduces the problem set-up, the conventional LSM, and an example of a directional scatterer which emphasizes the importance of the selection of suitable test dipole. Section 3 presents the first method, which we concisely refer to as LSM-L (where the trailing L stands for the regularization parameter L used in the proposed method). Section 4 presents the second method, which shall be called MLSM-L (first letter M represents the word 'multipoles' and the trailing L stands for the regularization parameter L). Section 5 presents several examples of dielectric scatterers and the reconstruction results of both the methods and Section 6 concludes the article.

2. THE PROBLEM SETUP AND LINEAR SAMPLING METHOD

2.1. The Problem Setup

We consider two dimensional vectorial electromagnetic inverse scattering problem of dielectric scatterers. We assume the longitudinal direction to be $\hat{z}$. The electric fields are restricted to the x-y plane and the magnetic fields are restricted to the longitudinal direction $\hat{z}$. This case corresponds to the transverse electric (TE) case. The measurement circle on which the receivers and transmitters

are located is denoted by Γ. The transmitters are two-dimensional electric dipoles of orientation $\vec{p}(\vec{r}_s) = p_{x,s}\hat{x} + p_{y,s}\hat{y}$; $s = 1$ to N_s where N_s is the number of transmitters. The detectors detect the scattered magnetic fields, $H_z(\vec{r}_d)\hat{z}$; $d = 1$ to N_d, where N_d is the number of detectors. In reality, the detectors often detect the electric fields. However, it is assumed for simplicity that the magnetic fields $H_z(\vec{r}_d)\hat{z}$ can be computed using Maxwell's equations. The domain of investigation is denoted by Ω and the scatterer support is denoted by Θ. The scatterer support is completely enclosed in the investigation domain, i.e., $\Theta \subset \Omega$.

We write the multistatic response matrix (MSR) $\mathbf{K}$ in the TE case as the mapping from the electric dipoles at the transmitters to the z-directed magnetic fields at the receivers:

$$\bar{H} = \mathbf{K} \cdot \bar{P}, \tag{1}$$

where $\bar{H} = [H_z(\vec{r}_{d=1})\ H_z(\vec{r}_{d=2})\ \ldots\ H_z(\vec{r}_d)\ \ldots\ H_z(\vec{r}_{N_d})]^T$, and $\bar{P} = [p_{x,1}\ p_{y,1}\ p_{x,2}\ p_{y,2}\ \ldots p_{x,N_s}\ p_{y,N_s}]^T$.

2.2. Linear Sampling Method

In the linear sampling method, the aim is to find a source current distribution $\bar{P}_{\mathrm{LSM}}$ such that:

$$\mathbf{K} \cdot \bar{P}_{\mathrm{LSM}} = \left[\ \bar{\phi}_x(\vec{r}) \quad \bar{\phi}_y(\vec{r})\ \right] \cdot \vec{q}(\vec{r}), \tag{2}$$

$$\vec{q}(\vec{r}) = q_x(\vec{r})\,\hat{x} + q_y(\vec{r})\,\hat{y} \tag{3}$$

where $\vec{r} \in \Omega$ is a sampling point in the domain of investigation. The elements in the vectors $\bar{\phi}_x(\vec{r})$ and $\bar{\phi}_y(\vec{r})$ are $\phi_x(\vec{r}_d, \vec{r})$, $d = 1$ to N_d and $\phi_y(\vec{r}_d, \vec{r})$, $d = 1$ to N_d, respectively, and $q_x(\vec{r})$ and $q_y(\vec{r})$ are the dipole moments of the hypothetical dipole sources chosen by the user for applying LSM. For convenience, $\vec{q}(\vec{r})$ is referred to as the 'test source'. Here, $\phi_x(\vec{r}_d, \vec{r})$ and $\phi_y(\vec{r}_d, \vec{r})$ are the radiation at a detector location $\vec{r}_d$ due to a unit x-directed and y-directed dipole respectively located at the sampling point $\vec{r}$ and are given by:

$$\phi_x\left(\vec{r}', \vec{r}\right) = k\mathrm{H}_1^{(1)}\left(k\left|\vec{r}' - \vec{r}\right|\right)\sin\theta_{(\vec{r}'-\vec{r})} \tag{4}$$

$$\phi_y\left(\vec{r}', \vec{r}\right) = -k\mathrm{H}_1^{(1)}\left(k\left|\vec{r}' - \vec{r}\right|\right)\cos\theta_{(\vec{r}'-\vec{r})} \tag{5}$$

According to the theory of the LSM, if the sampling point belongs to the scatterer support, i.e., $r \in \Theta$, then $\left|\bar{P}_{\mathrm{LSM}}\right|$ is finite, where $|\cdot|$ denotes the Euclidean norm. On the other hand, if the sampling point does not belong to the scatterer support, $r \notin \Theta$, then $|\bar{P}_{\mathrm{LSM}}|$ is not finite. In the case of noisy measurements of the scattered field, if $r \notin \Theta$, then $|\bar{P}_{\mathrm{LSM}}|$ is not infinite but large valued. Thus, traditionally either $|\bar{P}_{\mathrm{LSM}}|^{-1}$ or $-\log_{10}|\bar{P}_{\mathrm{LSM}}|$ is used as a pseudospectrum for estimating the scatterer support. In this paper, we have used $-\log_{10}|\bar{P}_{\mathrm{LSM}}|$ as the pseudospectrum.

2.3. Choice of the Test Source

As mentioned in the introduction, usually the test dipole $\vec{q}(\vec{r})$ is chosen as either $\vec{q}(\vec{r}) = \hat{x}$ or $\vec{q}(\vec{r}) = \hat{y}$ [4, 27]. As a result of this choice, the pseudospectrum of the LSM has a directional nature. For example, if $\vec{q}(\vec{r}) = \hat{y}$ is chosen, the features along the $\hat{y}$ direction are reconstructed better than the features along the $\hat{x}$ direction.

It was shown in [21] that though LSM uses a linear operator equation unlike the non-linear operator equations of scattering, there is a relationship between the two mathematical models. The relationship can be stated in as follows: Consider the expansion of the induced current distribution at a sampling point. LSM works if the test source used in LSM is a linear combination of the independent components of the effective current source at the sampling point.

Thus, if the effective source has no $\hat{y}$ component (and only $\hat{x}$ component) at a sampling point, LSM cannot detect that sampling point as scatterer support using $\vec{q}(\vec{r}) = \hat{y}$, irrespective of the true nature of the sampling point. The sampling point can be detected only if $\vec{q}(\vec{r}) = \hat{x}$ is used. Consider for example, a line type scatterer made of perfect electric conductor (PEC) of length 0.9λ placed along the x-axis. Since the scatterer is PEC, the currents are only along the boundary of the scatterer. It is expected that only $\vec{q}(\vec{r}) = \hat{x}$ is able to reconstruct the scatterer. This is confirmed in Figs. 1(a), (b), where it is seen that LSM with $\vec{q}(\vec{r}) = \hat{x}$ (Fig. 1(a)) and $\vec{q}(\vec{r}) = \hat{y}$ (Fig. 1(b)). We note that $N_s = N_d = 30$ have been used and the transmitters and receivers are distributed uniformly over a circle of radius 10λ. If

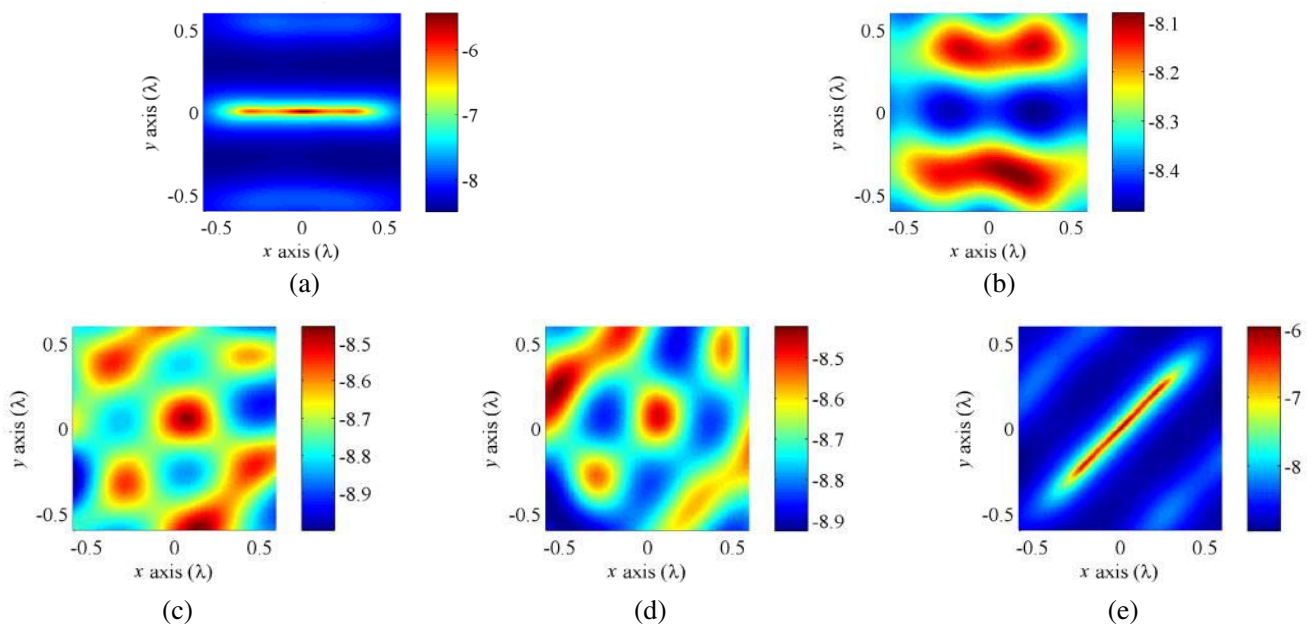

Figure 1. Imaging of line type PEC scatterer using conventional LSM. (a) LSM using $\vec{q}(\vec{r}) = \hat{x}$ for horizontal PEC. (b) LSM using $\vec{q}(\vec{r}) = \hat{y}$ for horizontal PEC. (c) LSM using $\vec{q}(\vec{r}) = \hat{x}$ for inclined PEC. (d) LSM using $\vec{q}(\vec{r}) = \hat{y}$ for inclined PEC. (e) LSM using $\vec{q}(\vec{r}) = (\hat{x} + \hat{y})/\sqrt{2}$ for inclined PEC.

the scatterer is inclined by 45°, LSM with neither $\vec{q}(\vec{r}) = \hat{x}$ (Fig. 1(c)) nor $\vec{q}(\vec{r}) = \hat{y}$ (Fig. 1(d)) can reconstruct the scatterer. Only LSM with $\vec{q}(\vec{r}) = (\hat{x} + \hat{y})/\sqrt{2}$ can reconstruct the scatterer (Fig. 1(e)).

There is an additional challenge for the dielectric scatterers. The direction of the induced current is different for different directions of incidences. Also, the induced current at a sampling point is related to the induced current distribution on the complete scatterer support, which is an unknown for the inverse problem. Thus, an optimal test direction selection is a very challenging problem and it is difficult to choose a suitable test direction using the physics of scattering.

Ideally, we may try infinitely many combinations of q_x and q_y and choose the results that look most reliable. However, such a choice has to be heuristic and there is no way to conclude if the chosen result is closest to the actual scatterer profile. Further, such an endeavour would entail huge amount of computation resources. On the other hand, several researchers prefer a combination of the pseudospectrums obtained using $\vec{q}(\vec{r}) = \hat{x}$ and $\vec{q}(\vec{r}) = \hat{y}$ [4, 27]. In the following two sections, Section 3 and Section 4, we propose two methods for the automatic selection of the test dipole $\vec{q}(\vec{r})$.

3. METHOD 1: NUMERICALLY ROBUST TEST DIRECTION

3.1. The Proposed Method

We revisit the operator equation of LSM given by (2). In this method, the aim is to select $\vec{q}(\vec{r})$ such that $|\bar{P}_{\mathrm{LSM}}|$ is numerically stable. For this purpose, we propose that $\vec{q}(\vec{r})$ can be chosen using the first few singular values of the MSR $\mathbf{K}$. It is well known that the first few singular vectors represent the most stable portion of the range space of $\mathbf{K}$ and the subspace spanned by the trailing singular values is most likely to be corrupted by the presence of noise. Thus, if $\vec{q}(\vec{r})$ is computed using the first few singular vectors of $\mathbf{K}$, then $\mathbf{K}$ is less likely to be affected by the presence of noise.

Using the derivation presented in [29], $\vec{q}(\vec{r})$ is chosen as the eigenvector corresponding to the maximum eigenvalue of $\mathbf{A}$, where:

$$\mathbf{A} = \left(\mathbf{G}\left(\vec{r}\right)^* \cdot \mathbf{G}\left(\vec{r}\right)\right)^{-1} \left(\left[\mathbf{U} \cdot \mathbf{G}\left(\vec{r}\right)\right]^* \cdot \left[\mathbf{U} \cdot \mathbf{G}\left(\vec{r}\right)\right]\right) \tag{6}$$

$$\mathbf{G}\left(\vec{r}\right) = \begin{bmatrix} \bar{\phi}_x & \bar{\phi}_y \end{bmatrix} \tag{7}$$

$$\mathbf{U} = [\ u_1 \quad \ldots \quad u_L\ ]^* \tag{8}$$

where $u_l,\ l = 1$ to L are the first L singular values of the MSR $\mathbf{K}$. Here, L behaves as a regularization parameter. For convenience, we refer to this method as LSM-L.

3.2. Relationship of the Proposed Method with the Test Dipole Selection for MUSIC [29]

As highlighted in Section 3.1, the proposed method uses the derivation in [29] for computing $\vec{q}(\vec{r})$. In this context, it is important to highlight the difference between the proposed method and [29]. We note that the work in [29] was developed for multiple signal classification (MUSIC) algorithm, which has an imposition on the degree of freedom of the scatterers. MUSIC is applicable for scatterers that are small in comparison to the wavelength λ and MUSIC mandates that the number of induced sources on the scatterers is less than the dimension of the MSR $\mathbf{K}$. Due to this imposition, the size of the range is directly linked to the number of dipoles induced on the scatterers. The mapping from the induced dipoles to the MSR matrix $\mathbf{K}$ is one-to-one. Further, the range of the MSR $\mathbf{K}$ is smaller than the dimension of the MSR $\mathbf{K}$ (i.e., MSR $\mathbf{K}$ is rank deficient) and this enables a clear segregation of the signal (range) subspace and the noise subspace. As a consequence, it is simple to choose the regularization parameter L in noise free as well as most noisy scenarios in MUSIC.

On the other hand, LSM deals with extended scatterers (not small in comparison to the wavelength λ). The induced currents are in the form of continuous distribution over a scatterer, and the mapping from the induced current distribution to the MSR $\mathbf{K}$ is not one-to-one. Moreover, the MSR $\mathbf{K}$ is full ranked and it is more difficult to choose the regularization parameter L in this case. Despite this, we highlight that some practical guidelines can be derived for choosing the regularization parameter L in the case of noisy measurements.

3.3. The Regularization Parameter L

Let $\sigma_l,\ l = 1$ to $\min(N_d, N_s)\,;\ \sigma_l > \sigma_{l+1} \forall l$ are the singular values of the MSR $\mathbf{K}$. A plot of the $\log_{10}\sigma_l$ is useful for selecting the regularization parameter L. The general guideline for the selection of the regularization parameter L is as follows:

1. If the plot of $\log_{10}\sigma_l$ has an initial flat region, then the value of l corresponding to the location from where the value of $\log_{10}\sigma_l$ starts dropping fast is chosen as the regularization parameter L.
2. If the plot of $\log_{10}\sigma_l$ has no initial flat region, then $L = 1$ is chosen.

Although the above is just a useful guidance, sometimes higher values of L may also give some reasonable reconstruction results. We acknowledge that a more robust and theoretically grounded method of choosing the regularization parameter L is needed and we hope that such method can be derived in the near future. We present two examples for demonstrating the effect of the regularization parameter L. For both the examples, the domain size is $1.2\lambda \times 1.2\lambda$ and $N_s = N_d = 30$ have been used. The transmitters and receivers are distributed uniformly over a circle of radius 10λ.

Example 1: The first example is an asymmetric scatterer with the shape of a '+' sign and relative permittivity 2. Each arm of the scatterer is of length 0.9λ and width 0.05λ. In a hypothetical domain $\widetilde{XY}$, the center of the scatterer is placed at $(0.1\lambda, 0.1\lambda)$. Then $\widetilde{XY}$ is rotated by an angle $\varphi = 60^\circ$ to obtain the actual domain XY. This is illustrated in Fig. 2.

First, the case of MSR $\mathbf{K}$ with 20 dB SNR is considered. The values of $\log_{10}\sigma_l$ are plotted in Fig. 3(a). It is seen that the plot of $\log_{10}\sigma_l$ is flat till $l = 2$. Hence, the condition 1 of the Section 3.3 is satisfied. The LSM pseudospectrums computed using the proposed method LSM-L for $L = 1$, 2, and 4 are plotted in Figs. 3(b)–(d) respectively. It is seen that the scatterer is reconstructed poorly using $L = 1$ (Fig. 3(b)). The scatterer can be reconstructed using $L = 2$ determined by the condition 1 (Fig. 3(c)). However, as stated earlier that in some cases, a higher value of L can also reconstruct the scatterer well, such a case is verified in Fig. 3(d) which uses $L = 4$.

Second, the case of MSR $\mathbf{K}$ with 10 dB SNR is considered. The values of $\log_{10}\sigma_l$ are plotted in Fig. 4(a) and the nature of first few singular values is similar to that in Fig. 3(a). It is seen that the plot of $\log_{10}\sigma_l$ is flat till $l = 2$. Hence, the condition 1 of Section 3.3 is satisfied. The LSM pseudospectrums computed using the proposed method LSM-L for $L = 1$, 2, and 4 are plotted in

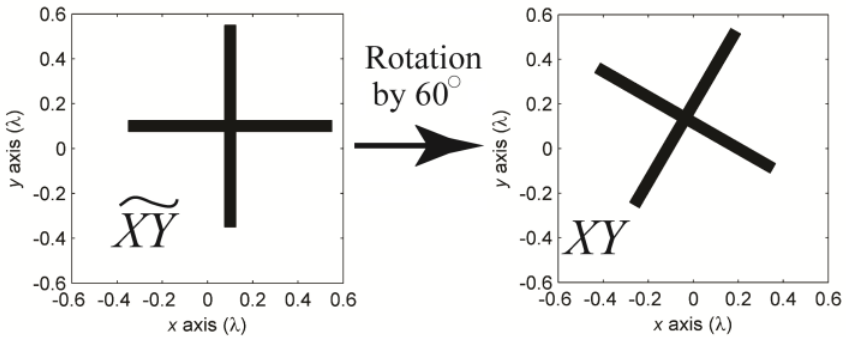

Figure 2. Demonstration of the hypothetical and actual domains of example 1 in Section 3.3.

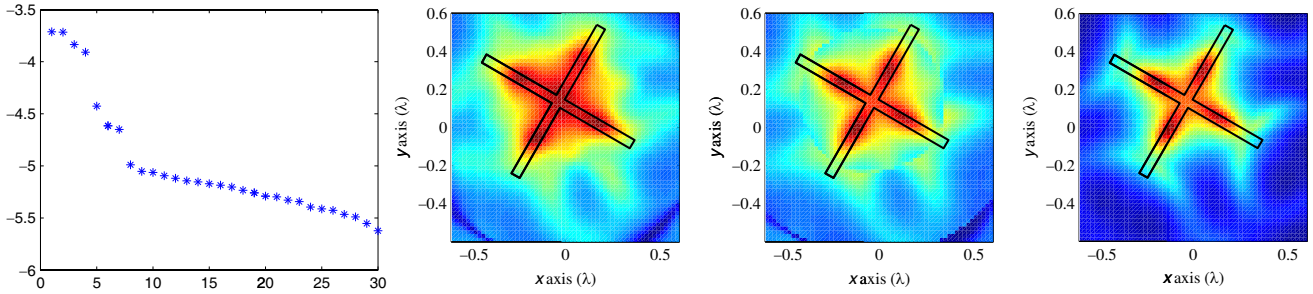

Figure 3. Demonstration of the regularization parameter L for method 1 (Section 3) for example 1 in 20 dB SNR. (a) The plot of singular values $\log_{10}\sigma_l$ shows that the singular values start trailing after the 7th singular values. (b) LSM-L for $L = 1$ (black line shows the contour of the scatterer). (c) LSM-L for $L = 2$ (black line shows the contour of the scatterer). (d) LSM-L for $L = 4$ (black line shows the contour of the scatterer).

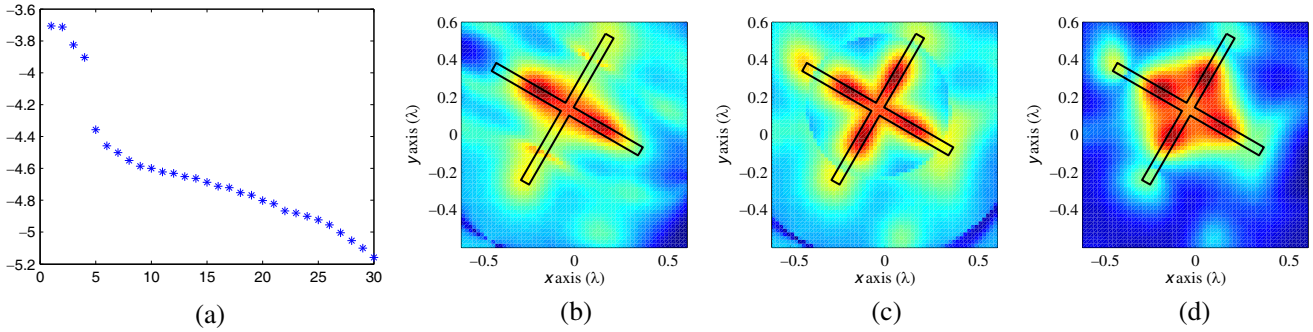

Figure 4. Demonstration of the regularization parameter L for method 1 (Section 3) for example 1 in 10 dB SNR. (a) The plot of singular values $\log_{10}\sigma_l$ shows that the singular values start trailing after the 4th singular values. (b) LSM-L for $L = 1$ (black line shows the contour of the scatterer). (c) LSM-L for $L = 2$ (black line shows the contour of the scatterer). (d) LSM-L for $L = 4$ (black line shows the contour of the scatterer).

Figs. 4(b)–(d) respectively. It is seen that the scatterer cannot be reconstructed using $L = 1$ (Fig. 4(b)). The scatterer can be reconstructed using $L = 2$ determined by the condition 1 (Fig. 4(c)). From Fig. 4(d), it is seen that $L = 4$ cannot reconstruct the scatterer in the case of 10 dB SNR.

Example 2: The second example is that of two circular scatterers, each of diameter 0.2λ and relative permittivity 2, placed symmetrically along the x-axis with their centers 0.5λ apart. First, the

case of MSR **K** with 20 dB SNR is considered. The relevant plots are presented in Fig. 5. It is seen in Fig. 5(a) that the values of $\log_{10}\sigma_l$ descend very fast for first few values of l and the remaining plot of $\log_{10}\sigma_l$ corresponding to $l > 7$ is relatively flat. This flat region corresponds to the corruption of the MSR **K** with noise. Due to the rapidly falling values of $\log_{10}\sigma_l$ for the initial values of l, condition 2 is applicable and thus $L = 1$ is a suitable choice. It is seen in Fig. 5(b) that the pseudospectrum corresponding to $L = 1$ can resolve the two scatterers, though the reconstructed scatterer support is slightly shifted from the actual scatterer support. The shift is attributed to strong coupling between the two scatterers owing to very small distance between them. On the other hand, the pseudospectrum corresponding to $L = 2$ shown in Fig. 5(c) cannot resolve the two scatterers.

Similar observation can be made for the case of 10 dB SNR, the figures of which are presented in Fig. 6. Condition 2 for the choice of the regularization parameter is applicable as seen from the plot of $\log_{10}\sigma_l$ in Fig. 6(a), and the two scatterers can be resolved in Fig. 6(b) which corresponds to $L = 1$. On the other hand, the scatterers cannot be resolved using $L = 2$, as seen in Fig. 6(c).

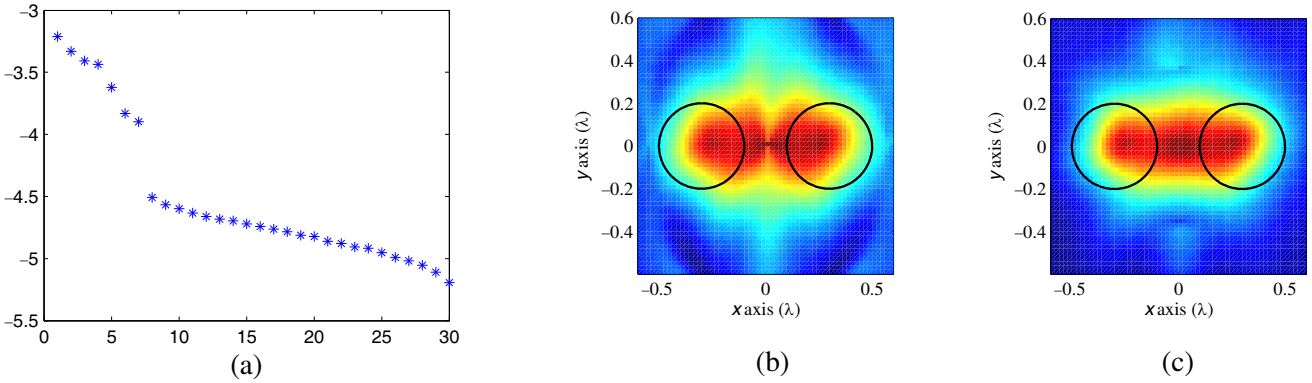

Figure 5. Demonstration of the regularization parameter L for method 1 (Section 3) for example 2 in 20 dB SNR. (a) The plot of singular values $\log_{10}\sigma_l$ shows that the singular values start trailing after the 7th singular values. (b) LSM-L for $L = 1$ (black line shows the contour of the scatterer). (c) LSM-L for $L = 2$ (black line shows the contour of the scatterer).

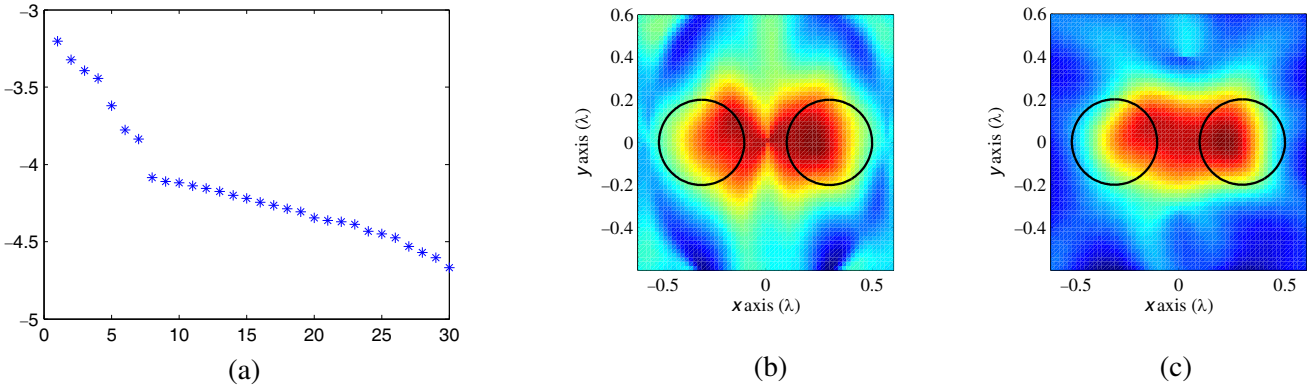

Figure 6. Demonstration of the regularization parameter L for method 1 (Section 3) for example 2 in 10 dB SNR. (a) The plot of singular values $\log_{10}\sigma_l$ shows that the singular values start trailing after the 7th singular values. (b) LSM-L for $L = 1$ (black line shows the contour of the scatterer). (c) LSM-L for $L = 2$ (black line shows the contour of the scatterer).

4. METHOD 2: MULTIPOLES BASED SELECTION OF TEST DIPOLE

4.1. The Proposed Method

It can be shown that the z-directed magnetic field due to a dipole in the transverse plane can be represented using a combination of two multipoles corresponding to $n = \pm 1$. Based on this derivation, we note that the magnetic field due to the dipole $\vec{q}(\vec{r})$ in right hand side of (2), i.e., $\left[\begin{array}{cc} \bar{\phi}_x(\vec{r}) & \bar{\phi}_y(\vec{r}) \end{array}\right] \cdot \vec{q}(\vec{r})$ can be represented using the radiation due to multipoles $n = \pm 1$. Thus, the mathematical model of the LSM given by (2) and (3) can be rewritten as:

$$\mathbf{K} \cdot \bar{P}_{\mathrm{MLSM}} = \left[\begin{array}{cc} \bar{\phi}_{-1}(\vec{r}) & \bar{\phi}_1(\vec{r}) \end{array}\right] \cdot \bar{b}(\vec{r}), \tag{9}$$

$$\bar{b}(\vec{r}) = \left[\begin{array}{cc} b_{-1}(\vec{r}) & b_1(\vec{r}) \end{array}\right]^T \tag{10}$$

where the elements in the vectors $\bar{\phi}_{-1}(\vec{r})$ and $\bar{\phi}_1(\vec{r})$ are $\phi_{-1}(\vec{r}_d, \vec{r})$, $d = 1$ to N_d and $\phi_1(\vec{r}_d, \vec{r}), d = 1$ to N_d respectively, and $b_{-1}(\vec{r})$ and $b_1(\vec{r})$ are the coefficients of the multipole currents. For convenience, $\bar{b}(\vec{r})$ is referred to as the 'multipole test source'. Here, $\phi_{-1}(\vec{r}_d, \vec{r})$ and $\phi_1(\vec{r}_d, \vec{r})$ are the multipole radiation functions corresponding to $n = -1$ and 1 at a detector location $\vec{r}_d$ and the sampling point $\vec{r}$. Their expressions are given by:

$$\phi_n(\vec{r}, \vec{r}\,') = \frac{i}{4} H_n^{(1)}\left(k\left|\vec{r} - \vec{r}\,'\right|\right) \exp\left(in \arg\left(\vec{r} - \vec{r}\,'\right)\right) \tag{11}$$

The development of multipoles based linear sampling method (MLSM) is similar to [21], with an important difference in the choice of the number of multipoles. The expression of the z-directed scattered magnetic field at a detector $H_z(\vec{r}_d, \vec{r}_s)$ can be expanded in terms of various multipoles corresponding to a sampling point $\vec{r}$ as:

$$H_z(\vec{r}_d, \vec{r}_s) = \sum_{n=-\infty}^{\infty} J_n(\vec{r}, \vec{r}_s) \phi_n(\vec{r}_d, \vec{r}) \tag{12}$$

In practice, the rigorous formulation of (12) can be simplified using a finite number of multipoles as follows:

$$H_z(\vec{r}_d, \vec{r}_s) \approx \sum_{n=-N}^{N} J_n(\vec{r}, \vec{r}_s) \phi_n(\vec{r}_d, \vec{r}) \tag{13}$$

where N is sufficiently large. Thus, the MSR $\mathbf{K}$ is expressed as:

$$\mathbf{K} = \mathbf{G}^{\mathrm{mul}} \cdot \mathbf{J}^{\mathrm{mul}} \tag{14}$$

where, $\mathbf{G}^{\mathrm{mul}}$ is a $N_d \times (2N+1)$ dimensional matrix containing the multipole radiation terms $\phi_n(\vec{r}_d, \vec{r})$, and $\mathbf{J}^{\mathrm{mul}}$ is a $(2N+1) \times N_s$ dimensional matrix, contains the effective multipole currents $J_n(\vec{r}, \vec{r}_s)$. $\mathbf{J}^{\mathrm{mul}}$ can be solved using least squares pseudoinverse.

In addition, term on the right hand side of (9) can be rewritten as follows:

$$\left[\begin{array}{cc} \bar{\phi}_{-1}(\vec{r}) & \bar{\phi}_1(\vec{r}) \end{array}\right] \cdot \bar{b}(\vec{r}) = \mathbf{G}^{\mathrm{mul}} \cdot \bar{D}, \tag{15}$$

where $\bar{D}(\vec{r})$ is a vector of dimension $(2N+1)$ and is given as follows:

$$\bar{D} = \left[\begin{array}{ccccccccc} 0 & \ldots & 0 & b_{-1}(\vec{r}) & 0 & b_1(\vec{r}) & 0 & \ldots & 0 \end{array}\right]^T \tag{16}$$

Then substituting (14) and (15), the mathematical model of LSM in (9) can be written as:

$$\mathbf{J}^{\mathrm{mul}} \cdot \bar{P}_{\mathrm{MLSM}} = \bar{D}(\vec{r}) \tag{17}$$

Then, using an approach similar to the approach presented in Section 3.1, the multipole test source $\bar{b}(\vec{r})$ is given as the eigenvector corresponding to the maximum eigenvalue of $\mathbf{B}$, where:

$$\mathbf{B} = \left(\mathbf{G}^{di}(\vec{r})^* \cdot \mathbf{G}^{di}(\vec{r})\right)^{-1} \left(\left[\mathbf{U} \cdot \mathbf{G}^{di}(\vec{r})\right]^* \cdot \left[\mathbf{U} \cdot \mathbf{G}^{di}(\vec{r})\right]\right) \tag{18}$$

$$\mathbf{G}^{di}(\vec{r}) = \left[\begin{array}{cc} \bar{\phi}_{-1} & \bar{\phi}_1 \end{array}\right] \tag{19}$$

and $\mathbf{U}$ is given by (8). Thus, through (8), MLSM is also connected to the regularization parameter L. So, we call the method proposed in this section as MLSM-L.

4.2. Algorithmic Summary and the Regularization Parameters

An algorithmic summary of the MLSM-L is presented below and the two regularization parameters are identified explicitly.

- Step 1: Compute the matrix $\mathbf{G}^{\text{mul}}$. Here, the first regularization parameter N comes into the picture.
- Step 2: Compute $\mathbf{J}^{\text{mul}}$ using (14). For computing $\mathbf{J}^{\text{mul}}$, either Moore Penrose pseudoinverse or truncated SVD based pseudoinverse may be used. We have used Moore Penrose pseudoinverse in this paper.
- Step 3: Compute $\mathbf{U}$ using (8). Here, the second regularization parameter L comes into the picture.
- Step 4: For each sampling point, do the following:
  - Step 4.1: Compute $\mathbf{G}^{di}(\vec{r})$ using (19).
  - Step 4.2: Compute $\mathbf{B}$ using (18) and $\bar{b}(\vec{r})$ using the eigenvector corresponding to the maximum eigenvalue of $\mathbf{B}$.
  - Step 4.3: Compute $\bar{D}(\vec{r})$ using (16).
  - Step 4.4: Compute $\bar{P}_{\text{MLSM}}$ using (17).

As identified in steps 1 and 3, there are two regularization parameters N and L. The effect of the regularization parameter L is the same for LSM-L and MLSM-L, and it can be chosen using the conditions 1 and 2 for the Section 3.3. The choice of the regularization parameter N is discussed in the next section.

4.3. Regularization Parameters N

The regularization parameter N indicates the number of multipoles chosen to approximate the z-directed scattered magnetic field $H_z(\vec{r}_d, \vec{r}_s)$ in (13). In [21], it was proposed that $N = 1$ is a good choice for the transverse magnetic case. This was based on the fact that the monopole currents ($n = 0$) are the most prominent multipoles in the transverse magnetic case and all other multipoles are negligibly small.

However, this is not true in the TE case. In the TE case, the dipoles (corresponding to $n = \pm 1$) are the most prominent dipoles. However, the other multipoles may not be negligibly small. This fact is illustrated using the examples presented in Section 3.3. For each sampling point in the domain and each incidence, the effective multipole currents $|\alpha_n(\vec{r}, \vec{r}_s)|$ are computed using (A6) (presented in the Appendix) for $n \in [-10, 10]$. For $n = 0$ to 10, the value of $\sum_{s=1}^{N_s} |\alpha_n(\vec{r}, \vec{r}_s)|$ is plotted in Fig. 7 and Fig. 8 for examples 1 and 2 respectively. In addition, $\beta_n = \max(\sum_{s=1}^{N_s} |\alpha_n(\vec{r}, \vec{r}_s)|; \forall \vec{r} \in \Omega)$ for $n \in [-10, 10]$ is also plotted for both the examples in last subfigures of Fig. 7 and Fig. 8.

It is seen that the dipoles $n = \pm 1$ are not the only prominent multipoles, but first several multipoles are significantly high. Thus, choosing only a few multipoles is not sufficient. A guideline for selecting the suitable value of N can be derived using the smallest circular scatterer that completely encloses the domain of interest and has the relative permittivity selected heuristically. Here, we choose its relative permittivity to be 2 and plot the scattering strengths of various multipoles using the derivation in [30] in Fig. 9. It is seen that the scattering strengths are negligible for $|n| > 10$. Thus, $N = 10$ is chosen as the regularization parameter.

5. EXAMPLES

In this section, we consider several examples and present the result of LSM-x (LSM with test source $\vec{q}(\vec{r}) = \hat{x}$), LSM-y (LSM with test source $\vec{q}(\vec{r}) = \hat{y}$), LSM-L, and MLSM-L (using $N = 10$). The relative permittivity of all the scatterers is 2. The size of the domain of interest is $1.2\lambda \times 1.2\lambda$ and $N_s = N_d = 30$ have been used. The transmitters and receivers are distributed uniformly over a circle of radius 10λ.

Examples 1 and 2 are the same examples as introduced in Section 3.3. Examples 3 and 4 are flower shaped scatterers, the boundaries of which are represented by:

$$\vec{r} = \frac{R}{b}\left(1 - b\sin(n\theta)\right)\left(\cos\theta\hat{x} + \sin\theta\hat{y}\right). \tag{20}$$

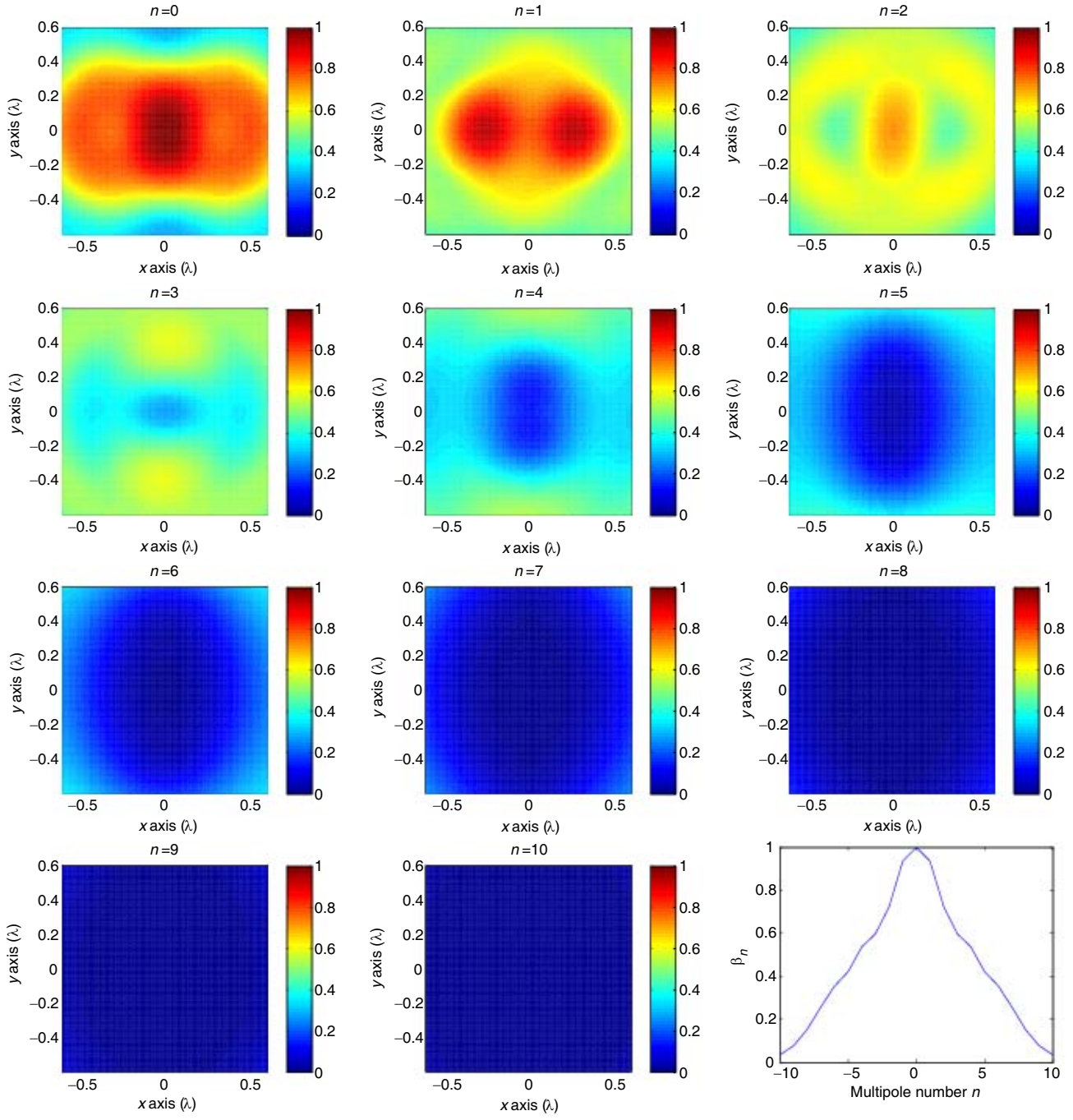

Figure 7. Plot of the effective multipole currents at various sampling points for the example 1.

The values of R and b are chosen as 0.5λ and 0.7, and examples 3 and 4 use $n = 3$ and 4, respectively.

Example 5 considers 2 elongated bar shaped scatterers placed parallel to each other. The bars are each of length 0.75λ and width 0.1λ. In the hypothetical domain $\widetilde{XY}$ similar to example 2, the locations of the bars are $(0, -0.4\lambda)$ and $(0, 0.4\lambda)$ respectively. The actual domain XY is obtained by rotating the hypothetical domain $\widetilde{XY}$ by $\varphi = 60^\circ$.

Example 6 considers 2 elongated bar shaped scatterers placed perpendicular to each other. The bars are each of length 0.6λ and width 0.1λ. In the hypothetical domain $\widetilde{XY}$ similar to example 2, the locations of the bars are $(0.14\lambda, -0.315\lambda)$ and $(-0.14\lambda, 0.315\lambda)$ respectively. The first bar is placed

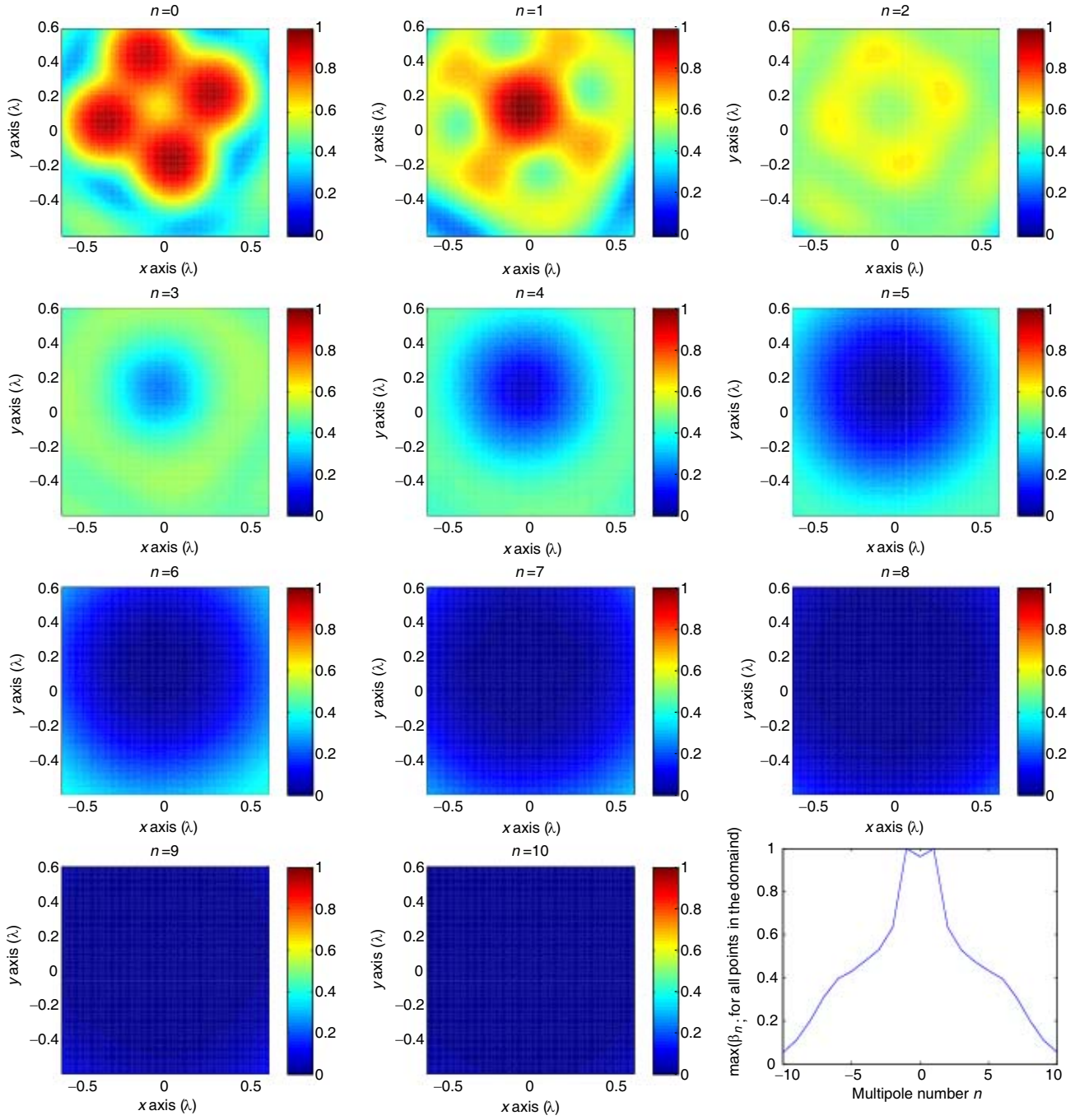

Figure 8. Plot of the effective multipole currents at various sampling points for the example 2.

horizontally and the second bar is placed vertically. The actual domain XY is obtained by rotating the hypothetical domain $\widetilde{XY}$ by $\varphi = 60°$.

The results for the case of 20 dB SNR are presented in Fig. 10–Fig. 15 for the examples 1–6 respectively. The results for the case of 10 dB SNR are presented in Fig. 16–Fig. 21 for the examples 1–6 respectively. In Fig. 10–Fig. 21, the outline of the actual scatterers is shown using black line.

For example 1, we see that LSM-x and LSM-y can roughly detect the scatterer shape in the case of 20 dB SNR (Figs. 10(a), (b)), but cannot detect the shape correctly in the case of 10 dB SNR (Figs. 16(a), (b)). In either case, the directional nature of LSM-x and LSM-y is clearly evident. On the other hand,

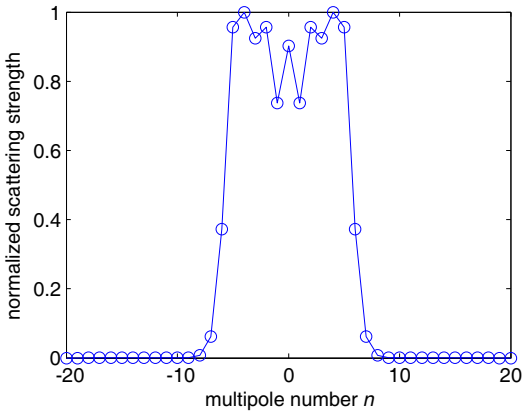

Figure 9. Plot of the scattering strengths corresponding to various multipoles for the smallest circular scatterer of relative permittivity 2 that completely encloses the domain of interest.

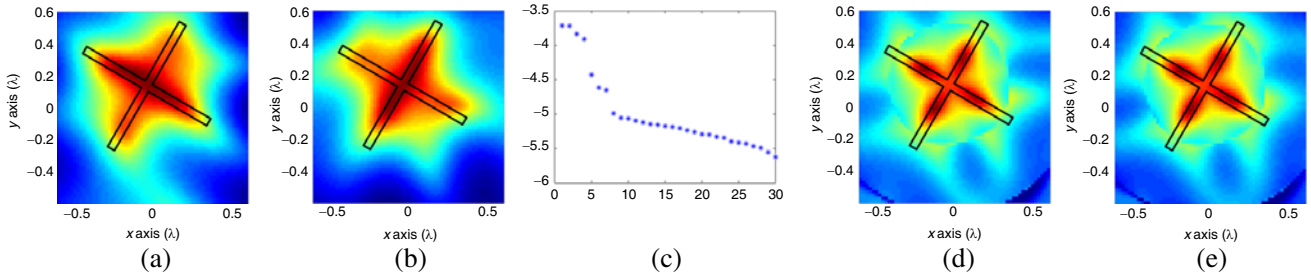

Figure 10. Comparison of various forms of LSM for example 1 (20 dB SNR). The black line represents the actual scatterer. (a) LSM-x. (b) LSM-y. (c) $\log_{10}$ (singular values). (d) LSM-L ($L = 2$). (e) MLSM-L ($L = 2$).

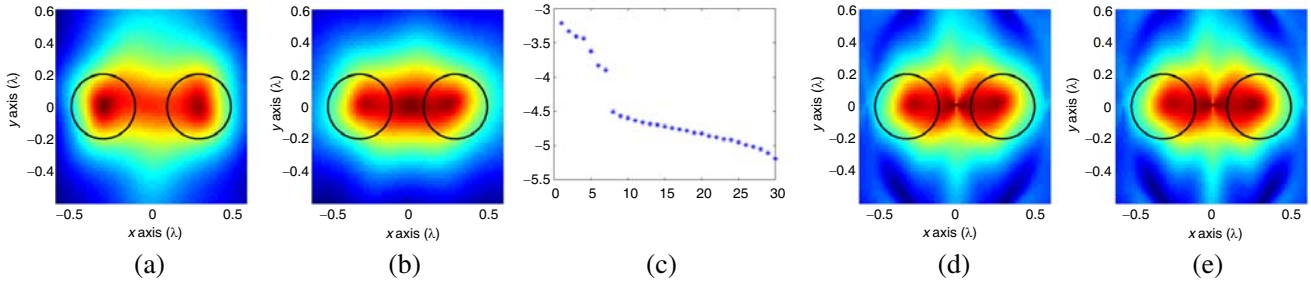

Figure 11. Comparison of various forms of LSM for example 2 (20 dB SNR). The black line represents the actual scatterer. (a) LSM-x. (b) LSM-y. (c) $\log_{10}$ (singular values). (d) LSM-L ($L = 1$). (e) MLSM-L ($L = 1$).

LSM-L and MLSM-L can detect the shape well (Figs. 10(d), (e) and Figs. 16(d), (e)).

For example 2 (Fig. 11 and Fig. 17), LSM-x and LSM-y cannot detect the presence of two circular scatterers and instead give an extended envelope encompassing both the scatterers. On the other hand, LSM-L and MLSM-L can detect the presence of two scatterers through a neck appearing between the two scatterers. Having said that, the scatterer support estimated by LSM-L and MLSM-L is more likely similar to a dumbbell and the position of the scatterers may be estimated incorrectly.

For the example 3 (Fig. 12 and Fig. 18) and 4 (Fig. 13 and Fig. 19), LSM-L and MLSM-L both can give a general idea of the scatterer through the envelope of the pseudospectrums (with three extensions and four extensions for the examples 3 and 4 respectively, in the correct directions). However, the

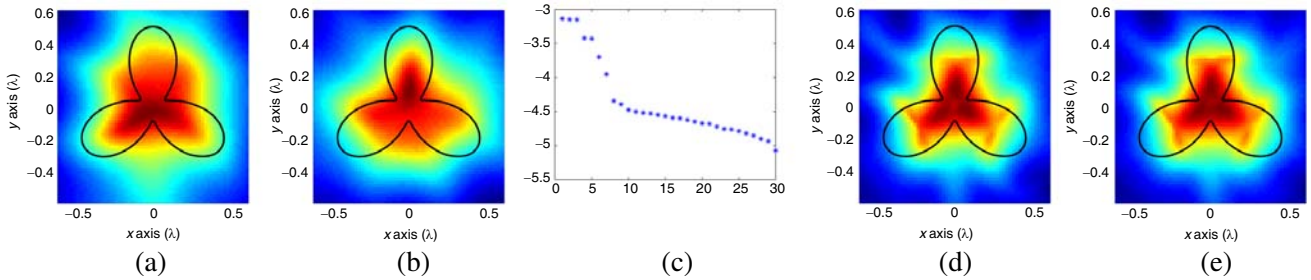

Figure 12. Comparison of various forms of LSM for example 3 (20 dB SNR). The black line represents the actual scatterer. (a) LSM-x. (b) LSM-y. (c) $\log_{10}$ (singular values). (d) LSM-L ($L = 3$). (e) MLSM-L ($L = 3$).

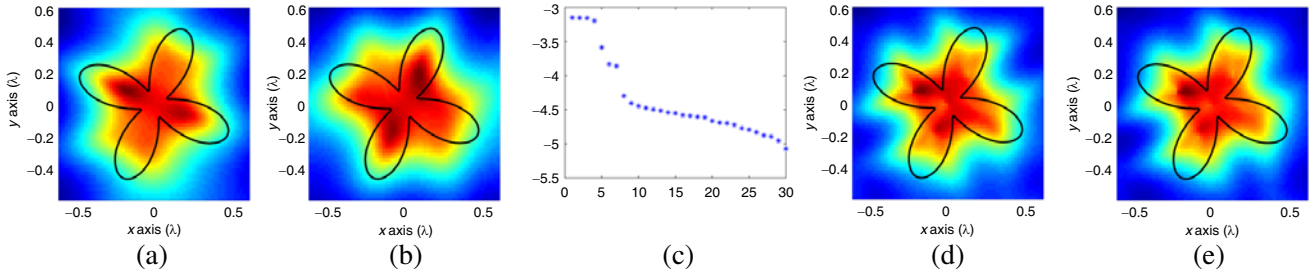

Figure 13. Comparison of various forms of LSM for example 4 (20 dB SNR). The black line represents the actual scatterer. (a) LSM-x. (b) LSM-y. (c) $\log_{10}$ (singular values). (d) LSM-L ($L = 3$). (e) MLSM-L ($L = 3$).

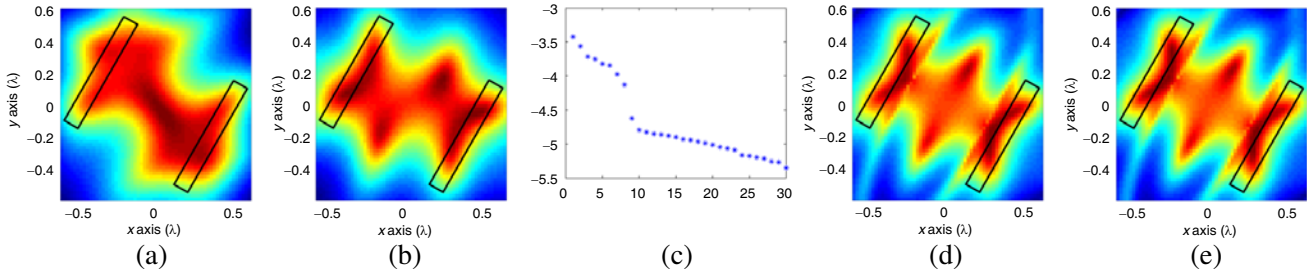

Figure 14. Comparison of various forms of LSM for example 5 (20 dB SNR). The black line represents the actual scatterer. (a) LSM-x. (b) LSM-y. (c) $\log_{10}$ (singular values). (d) LSM-L ($L = 1$). (e) MLSM-L ($L = 1$).

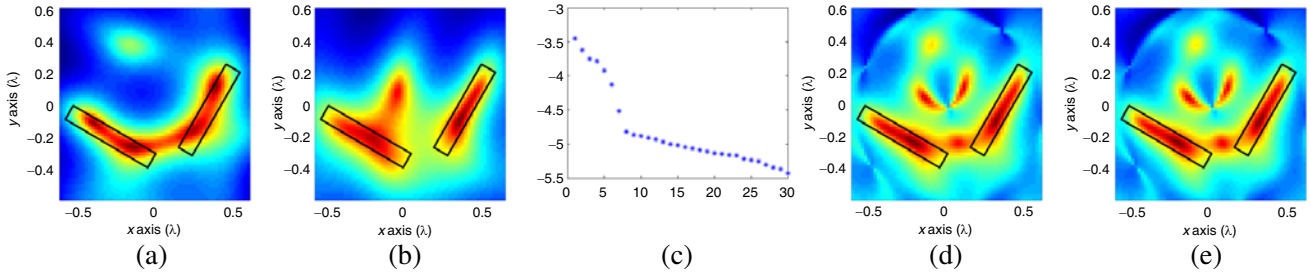

Figure 15. Comparison of various forms of LSM for example 6 (20 dB SNR). The black line represents the actual scatterer. (a) LSM-x. (b) LSM-y. (c) $\log_{10}$ (singular values). (d) LSM-L ($L = 1$). (e) MLSM-L ($L = 1$).

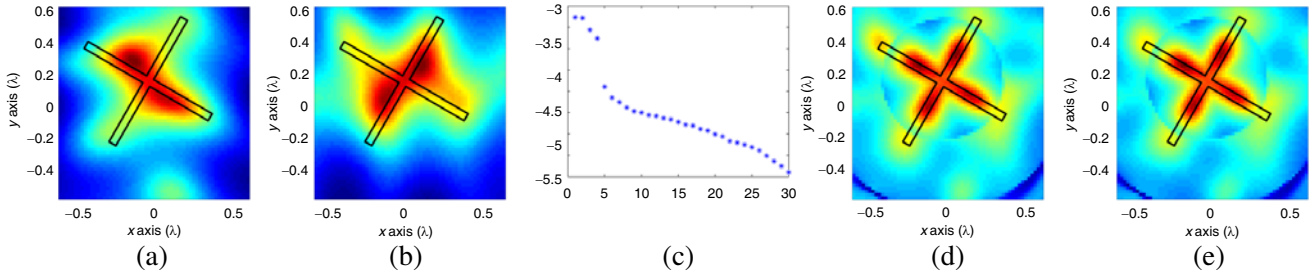

Figure 16. Comparison of various forms of LSM for example 1 (10 dB SNR). The black line represents the actual scatterer. (a) LSM-x. (b) LSM-y. (c) $\log_{10}$ (singular values). (d) LSM-L ($L = 2$). (e) MLSM-L ($L = 2$).

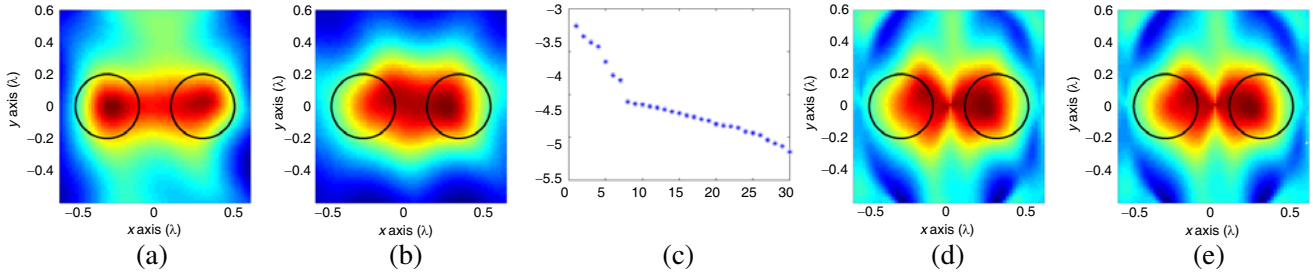

Figure 17. Comparison of various forms of LSM for example 2 (10 dB SNR). The black line represents the actual scatterer. (a) LSM-x. (b) LSM-y. (c) $\log_{10}$ (singular values). (d) LSM-L ($L = 1$). (e) MLSM-L ($L = 1$).

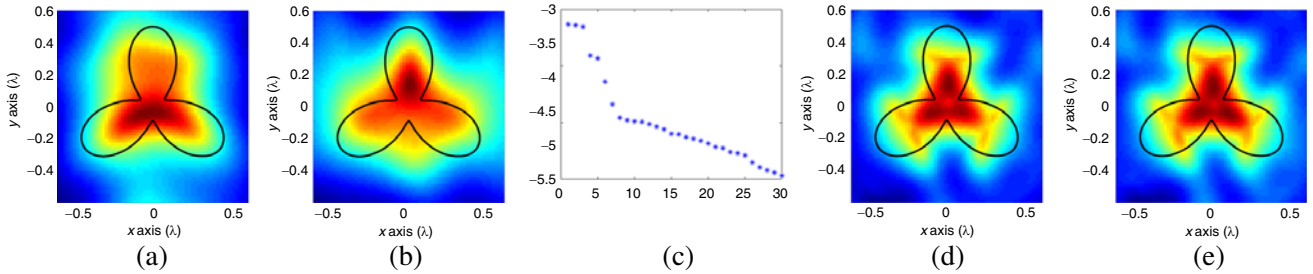

Figure 18. Comparison of various forms of LSM for example 3 (10 dB SNR). The black line represents the actual scatterer. (a) LSM-x. (b) LSM-y. (c) $\log_{10}$ (singular values). (d) LSM-L ($L = 3$). (e) MLSM-L ($L = 3$).

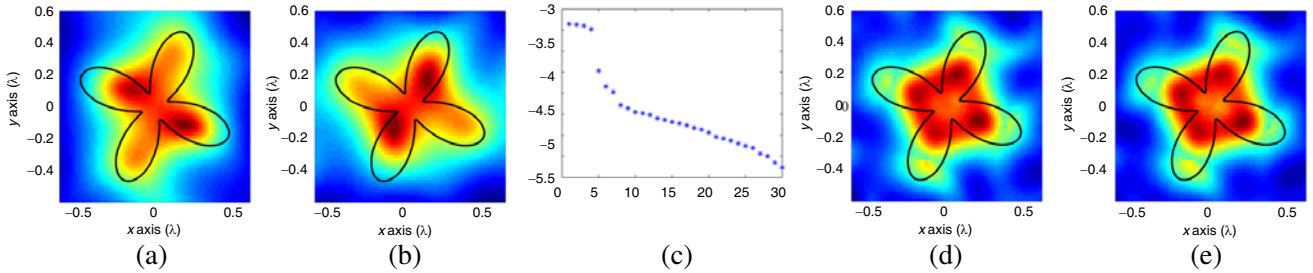

Figure 19. Comparison of various forms of LSM for example 4 (10 dB SNR). The black line represents the actual scatterer. (a) LSM-x. (b) LSM-y. (c) $\log_{10}$ (singular values). (d) LSM-L ($L = 4$). (e) MLSM-L ($L = 4$).

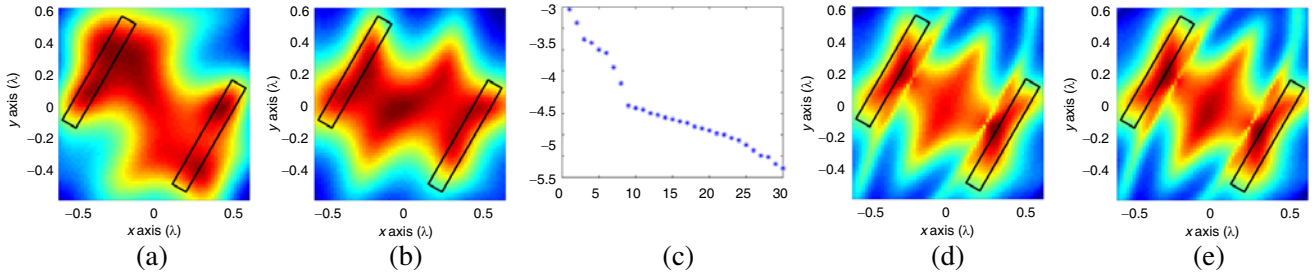

Figure 20. Comparison of various forms of LSM for example 5 (10 dB SNR). The black line represents the actual scatterer. (a) LSM-x. (b) LSM-y. (c) $\log_{10}$ (singular values). (d) LSM-L ($L = 1$). (e) MLSM-L ($L = 1$).

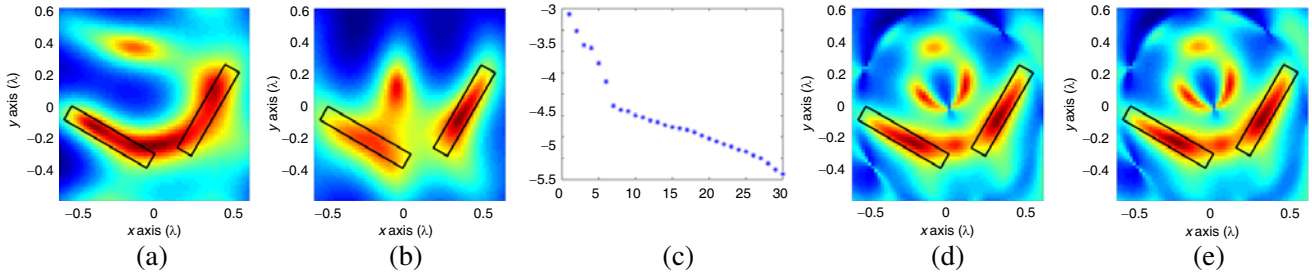

Figure 21. Comparison of various forms of LSM for example 6 (10 dB SNR). The black line represents the actual scatterer. (a) LSM-x. (b) LSM-y. (c) $\log_{10}$ (singular values). (d) LSM-L ($L = 1$). (e) MLSM-L ($L = 1$).

reconstruction of example 4 in 10 dB SNR is comparatively very poor. On the other hand, the extended arms of the envelopes of pseudospectrums for LSM-x and LSM-y are neither in the correct number nor in the correct directions.

In example 5 (Fig. 14 and Fig. 20), where two parallel bar shaped scatterers are considered, LSM-x and LSM-y detect a continuous blur envelope encompassing the two scatterers and the space between them. On the other hand, LSM-L and MLSM-L detect the presence of the two scatterers more accurately, though the pseudospectrum shown an artefact which may be confused as a third scatterer present symmetrically to both the scatterers. This artifact appears due to strong mutual coupling between the scatterers and causes the continuous envelope observed in LSM-x and LSM-y as well.

Finally, the directional nature of LSM-x and LSM-y is very strongly visible in example 6 (Fig. 15 and Fig. 21). LSM-x detects the left scatterer better (which makes a small angle with the x-axis) while LSM-y detects the right scatterer better (which makes a small angle with the y-axis). On the other hand the results of LSM-L and MLSM-L are rather symmetric. All four of them generate artifacts, with LSM-L and MLSM-L generating three small artifacts each as compared to one artifact each for LSM-x and LSM-y. However, the relative accuracy of detecting the scatterers is better for LSM-L and MLSM-L as compared to LSM-x and LSM-y.

6. CONCLUSION

Linear sampling method for reconstruction of extended scatterers in the transverse electric case is considered in this paper. The problem of the selection of the test dipole is addressed. Two methods are proposed to determine the test dipole automatically from the measurement data. Guidelines for the selection of the regularization parameters are also presented. Both the methods are essentially numerical and non-iterative. However, the first method is purely numerical and uses the numerically stable subspace of the multistatic response matrix for determining the direction of the test dipole. The second method takes into account the physics of the scattering as well by restricting the number of

multipoles that represent the scattered magnetic field. This indirectly means that we choose a small physical subspace of the scattered magnetic field that spans the radiation due to first few multipoles only. Then, we use the test dipole in this subspace of the scattered magnetic field only. The number of multipoles used for this purpose is determined using the largest sphere enclosing the domain of interest.

Several examples were considered for demonstrating the performance of the proposed method against the conventionally used either x or y-directed test dipoles. These examples are difficult to reconstruct using x or y-directed test dipoles or the images obtained from combining the reconstruction results for these dipoles. The proposed methods demonstrate better reconstruction results than the results of x or y-directed test dipoles.

Here, we note that both the methods and the reconstruction results serve to demonstrate the fact that suitably chosen test dipoles can significantly improve the reconstruction results and that the researchers should look beyond the conventional x or y-directed test dipoles for improving the performance of LSM. In the future, it will be interesting to consider answering some of the following questions. Can we design better techniques for choosing the test dipole more effectively and improving the reconstruction results? Will an iterative approach serve better? Instead of using the theory of multipoles, can some other physical bases prove more useful in improving the reconstruction results? Or should the dimension of physical subspace be chosen differently? Is such an approach specifically suitable or unsuitable to certain category of inverse scattering problems, like anisotropic scatterers, high contrast scatterers, or elongated scatterers? These are a few of the interesting questions that need to be answered in the near future. We hope that the current work will open new avenues in the research on the linear sampling method.

ACKNOWLEDGMENT

The author thanks Associate Professor Xudong Chen, National University of Singapore, for helpful discussions.

APPENDIX A.

In this section, we derive the effective multipole currents $\alpha_n(\vec{r}')$ at a sampling point $\vec{r}'$ due to an induced current distribution $\vec{I}(\vec{r} \in \Omega) = I_x(\vec{r})\hat{x} + I_y(\vec{r})\hat{y}$ in the domain of interest Ω. The current distribution induced due to the presence of the scatterers creates a z-directed magnetic field at the detectors:

$$H_z\left(\vec{r}_d\right) = \int\limits_{\vec{r}\in\Omega} \left(\phi_x\left(\vec{r}_d, \vec{r}\right) I_x\left(\vec{r}\right) + \phi_y\left(\vec{r}_d, \vec{r}\right) I_y\left(\vec{r}\right)\right) d\vec{r} \tag{A1}$$

where $\vec{I}(\vec{r} \in \Omega) = I_x(\vec{r})\hat{x} + I_y(\vec{r})\hat{y}$ and $\phi_x(\vec{r}_d, \vec{r})$ and $\phi_y(\vec{r}_d, \vec{r})$ are given by (4) and (5) respectively. Equation (A1) can be rewritten by substituting (4) and (5) and performing algebraic manipulations:

$$H_z\left(\vec{r}_d\right) = -2k \int\limits_{\vec{r}\in\Omega} \left(\phi_{-1}\left(\vec{r}_d, \vec{r}\right) a_{-1}\left(\vec{r}\right) + \phi_1\left(\vec{r}_d, \vec{r}\right) a_1\left(\vec{r}\right)\right) d\vec{r} \tag{A2}$$

$$a_{-1}\left(\vec{r}\right) = \left(I_x\left(\vec{r}\right) + iI_y\left(\vec{r}\right)\right); \quad a_1\left(\vec{r}\right) = \left(I_x\left(\vec{r}\right) - iI_y\left(\vec{r}\right)\right) \tag{A3}$$

where $\phi_{-1}\left(\vec{r}_d, \vec{r}\right)$ and $\phi_1\left(\vec{r}_d, \vec{r}\right)$ are given by (11). If the detectors are in the far field from the domain, then using the addition theorem [31] in the following form:

$$\phi_m\left(\vec{r}_d, \vec{r}\right) = \sum_{n=-\infty}^{\infty} \phi_{m-n}\left(\vec{r}_d, \vec{r}'\right) \mathrm{J}_n\left(k\left|\vec{r} - \vec{r}'\right|\right) \exp\left(-in \arg\left(\vec{r} - \vec{r}'\right)\right), \tag{A4}$$

Equation (A2) can be rewritten as:

$$H_z\left(\vec{r}_d\right) = \sum_{n=-\infty}^{\infty} \phi_n\left(\vec{r}_d, \vec{r}'\right) \alpha_n\left(\vec{r}'\right) \tag{A5}$$

where

$$\alpha_n\left(\vec{r}\,'\right) = \int\limits_{\vec{r}\in\Omega} \left\{ \mathrm{J}_{n+1}\left(k\left|\vec{r}-\vec{r}\,'\right|\right) \exp\left(-i\left(n+1\right)\arg\left(\vec{r}-\vec{r}\,'\right)\right) a_{-1}\left(\vec{r}\right) + \mathrm{J}_{n-1}\left(k\left|\vec{r}-\vec{r}\,'\right|\right) \exp\left(-i\left(n-1\right)\arg\left(\vec{r}-\vec{r}\,'\right)\right) a_{1}\left(\vec{r}\right) \right\} d\vec{r} \tag{A6}$$

are the desired effective multipole currents at the sampling point $\vec{r}\,'$.

REFERENCES

1. Colton, D. and R. Kress, "Using fundamental solutions in inverse scattering," *Inverse Problems*, Vol. 22, R49–R66, Jun. 2006.
2. Kirsch, A. and S. Ritter, "A linear sampling method for inverse scattering from an open arc," *Inverse Problems*, Vol. 16, 89–105, Feb. 2000.
3. Cakoni, F., D. Colton, and H. Haddar, "The linear sampling method for anisotropic media," *Journal of Computational and Applied Mathematics*, Vol. 146, 285–299, Sep. 2002.
4. Colton, D., H. Haddar, and P. Monk, "The linear sampling method for solving the electromagnetic inverse scattering problem," *SIAM Journal on Scientific Computing*, Vol. 24, 719–731, Jan. 2002.
5. Cakoni, F. and D. Colton, "The linear sampling method for cracks," *Inverse Problems*, Vol. 19, 279–295, Apr. 2003.
6. Collino, F., M. Fares, and H. Haddar, "Numerical and analytical studies of the linear sampling method in electromagnetic inverse scattering problems," *Inverse Problems*, Vol. 19, 1279–1298, Dec. 2003.
7. Colton, D., H. Haddar, and M. Piana, "The linear sampling method in inverse electromagnetic scattering theory," *Inverse Problems*, Vol. 19, S105–S137, Dec. 2003.
8. Arens, T., "Why linear sampling works," *Inverse Problems*, Vol. 20, 163–173, Feb. 2004.
9. Cakoni, F., M. Fares, and H. Haddar, "Analysis of two linear sampling methods applied to electromagnetic imaging of buried objects," *Inverse Problems*, Vol. 22, 845–867, Jun. 2006.
10. Gebauer, B., M. Hanke, and C. Schneider, "Sampling methods for low-frequency electromagnetic imaging," *Inverse Problems*, Vol. 24, 15007-18, 2008.
11. Hanke, M., "Why linear sampling really seems to work," *Inverse Problems and Imaging*, Vol. 2, 373–395, Aug. 2008.
12. Pelekanos, G., K. H. Leem, and V. Sevroglou, "A preconditioned linear sampling method in inverse acoustic obstacle scattering," *Journal of Computational Analysis and Applications*, Vol. 10, 453–464, Oct. 2008.
13. Chen, Q., H. Haddar, A. Lechleiter, and P. Monk, "A sampling method for inverse scattering in the time domain," *Inverse Problems*, Vol. 26, 085001, 2010.
14. Thánh, N. T. and M. Sini, "An analysis of the accuracy of the linear sampling method for an acoustic inverse obstacle scattering problem," *Inverse Problems*, Vol. 26, 015010, 2010.
15. Zeng, F., F. Cakoni, and J. Sun, "An inverse electromagnetic scattering problem for a cavity," *Inverse Problems*, Vol. 27, 125002, 2011.
16. Catapano, I., F. Soldovieri, and L. Crocco, "On the feasibility of the linear sampling method for 3D GPR surveys," *Progress In Electromagnetics Research*, Vol. 118, 185–203, 2011.
17. Scapaticci, R., L. Di Donato, I. Catapano, and L. Crocco, "Feasibility study on microwave imaging for brain stroke monitoring," *Progress In Electromagnetics Research B*, 305–324, 2012.
18. Shelton, N. and K. F. Warnick, "Behavior of the regularized sampling inverse scattering method at internal resonance frequencies," *Progress In Electromagnetics Research*, Vol. 38, 29–45, 2003.
19. Catapano, I., L. Crocco, and T. Isernia, "On simple methods for shape reconstruction of unknown scatterers," *IEEE Transactions on Antennas and Propagation*, Vol. 55, 1431–1436, May 2007.
20. Catapano, I., L. Crocco, and T. Isernia, "Linear sampling method: Physical interpretation and guidelines for a successful application," *PIERS Proceedings*, 1152–1156, Hangzhou, China, Mar. 24–28, 2008.

21. Agarwal, K., X. Chen, and Y. Zhong, "A multipole-expansion based linear sampling method for solving inverse scattering problems," *Optics Express*, Vol. 18, 6366–6381, Mar. 2010.
22. Agarwal, K. and X. Chen, "Multipoles-based linear sampling method: Impact of using multipole expansion," *Journal of Physics: Conference Series*, Vol. 290, 012001-1–8, 2011.
23. Aramini, R., G. Caviglia, A. Massa, and M. Piana, "The linear sampling method and energy conservation," *Inverse Problems*, Vol. 26, 055004, 2010.
24. Li, J., H. Liu, and Q. Wang, "Enhanced multilevel linear sampling methods for inverse scattering problems," *Journal of Computational Physics*, Vol. 257, 554–571, 2014.
25. Li, J., H. Liu, and J. Zou, "Strengthened linear sampling method with a reference ball," *SIAM Journal on Scientific Computing*, Vol. 31, 4013–4040, 2009.
26. Li, J., H. Liu, H. Sun, and J. Zou, "Reconstructing acoustic obstacles by planar and cylindrical waves," *Journal of Mathematical Physics*, Vol. 53, 2012.
27. Brignone, M., G. Bozza, A. Randazzo, M. Piana, and M. Pastorino, "A hybrid approach to 3D microwave imaging by using linear sampling and ACO," *IEEE Transactions on Antennas and Propagation*, Vol. 56, 3224–3232, Oct. 2008.
28. Chen, X. and K. Agarwal, "MUSIC algorithm for two-dimensional inverse problems with special characteristics of cylinders," *IEEE Transactions on Antennas and Propagation*, Vol. 56, 1808–1812, Jun. 2008.
29. Chen, X. and Y. Zhong, "MUSIC electromagnetic imaging with enhanced resolution for small inclusions," *Inverse Problems*, Vol. 25, Article No. 015008, Jan. 2009.
30. Rao, T. and X. Chen, "Analysis of the time-reversal operator for a single cylinder under two-dimensional settings," *Journal of Electromagnetic Waves and Applications*, Vol. 20, No. 15, 2153–2165, 2006.
31. Abramowitz, M. and I. A. Stegun, *Handbook of Mathematical Functions: with Formulas, Graphs, and Mathematical Tables*, 7th edition, Dover Publications, New York, 1972.